Smoothed particle hydrodynamics with diffusive flux for advection–diffusion equation with discontinuities

Computers and Mathematics with Applications 160 (2024) 70–85

Contents lists available at ScienceDirect

Computers and Mathematics with Applications

journal homepage: www.elsevier.com/locate/camwa

Smoothed particle hydrodynamics with diffusive flux for advection–diffusion equation with discontinuities

Zewei Sun [a], Qingzhi Hou [b,*], Arris S. Tijsseling [c], Jijian Lian [b], Jianguo Wei [a]

[a] College of Intelligence and Computing, Tianjin University, Tianjin 300350, China
[b] State Key Laboratory of Hydraulic Engineering Simulation and Safety, Tianjin University, Tianjin 300350, China
[c] Department of Mathematics and Computer Science, Eindhoven University of Technology, P.O. Box 513, Eindhoven 5600 MB, the Netherlands

ARTICLE INFO

Keywords:
Smoothed particle hydrodynamics
Advection-diffusion
Flux-form
Diffusive flux
Partial diffusive flux
Discontinuity

ABSTRACT

The advection-diffusion equation (ADE) with variable diffusion coefficient can be written in a flux form to avoid rewriting the diffusion term with a drift. However, for solving the flux-form ADE using smoothed particle hydrodynamics (SPH), a double first-order derivative approximation has to be used to approximate the diffusion term, which creates non-physical oscillations at any discontinuities. This is one reason why the flux-form diffusion is rarely used in SPH. To prevent such oscillations, the conditions and causes of them are theoretically analyzed, and a new partial diffusive flux format is proposed. To improve the particle consistency, a corrective particle approximation is applied. The effectiveness of the proposed method is verified by solving four ADE cases with analytical solutions. The results shown that SPH in partial diffusive flux can fully eliminate the spurious oscillations, and achieve second-order accuracy and second-order uniform convergence for contaminant transport problems with discontinuities. Moreover, compared with the conventional diffusive flux format, the numerical error of the proposed method is reduced by at least one order of magnitude. An encouraging possibility for the application of the smoothed particle hydrodynamics with diffusive flux to the anisotropic dispersion is also provided.

1. Introduction

The material transport process is often represented by an advection–diffusion equation (ADE) in many scientific engineering fields, such as sediment transport [1], oil spills [2], and salinity simulations [3]. The ADE typically has the form:

$$\frac{\partial c}{\partial t} + \vec{v} \cdot \nabla c = \nabla \cdot (D \nabla c), \tag{1}$$

where c is the concentration, $\vec{v}$ is the flow velocity and D is the diffusion coefficient. Numerical methods for solving the ADE remain the subject of extensive research in computational fluid dynamics [4]. As a Lagrangian meshless technique, the smoothed particle hydrodynamics (SPH) method has been applied to ADEs in various fields [5,6]. In the Lagrangian system, the dependent variables are a function of the initial position x and time t. Thus, the ADE may be written as:

$$\frac{\mathrm{d}\hat{c}}{\mathrm{d}t} = \nabla \cdot (D \nabla \hat{c}) \tag{2}$$

where $\hat{c}$ is the concentration of the tracer, $\mathrm{d}\hat{c}/\mathrm{d}t$ is the total derivative, and $\hat{x}$ is the Lagrangian position of the parcel at time t.

As a meshfree Lagrangian particle numerical technique, the SPH method was proposed by Gingold and Monaghan [7] and Lucy [8] independently in 1977, and it was historically aimed at solving the astrophysical problems. With an important extension to free-surface flows [9], it is now widely used in various fields [10,11]. In the field of hydrodynamics, its applications include suspended particle flows [12], reacting flows [13], and bioheat transfer [14]. By discretizing the governing equations from the functions of integration, the SPH realizes the approximation of the Lagrangian form. A key focus of solving the ADE with SPH is the approximation of the diffusion terms [15], for which there are essentially two approaches. One

* Corresponding author.
E-mail address: qhou@tju.edu.cn (Q. Hou).

https://doi.org/10.1016/j.camwa.2024.02.012
Received 18 August 2023; Received in revised form 10 December 2023; Accepted 3 February 2024

involves directly approximating the second-order diffusion terms using a Taylor series expansion, known as the difference scheme (DS) [5,15]. Various forms of the DS have been investigated for high-accuracy formulations [16] and GPU acceleration [17–19]. Using the acceleration of GPU, Hou et al. [20] applied the DS format to contaminant transport problems with discontinuities in groundwater and validated it against practical engineering cases. However, when the diffusion coefficient depends on the location or even concentration (like problems studied in [21–23]), the diffusion term has to be rewritten with an extra drift term $\nabla D \cdot \nabla c$. If the diffusion coefficient is related to other variables, such as velocity and pressure [24], the drift term will be more complicated. The second approach is to use a double first-order derivative approximation, known as the diffusive flux (DF) format [25]. This form is less common because non-physical oscillations may occur when the concentration is discontinuous [15,26]. Its higher computational cost is another drawback. When the diffusion coefficient is a function of space or even concentration, it is useful to apply the flux-form ADE to avoid rewriting the diffusion term as an ADE with a drift, rather than as a physical advection process [27]. The DF format is more suitable than the DS format for solving the flux-form ADE with SPH. Thus, a DF-based method without producing non-physical oscillations at discontinuities is highly needed. The contaminant transport in the natural is often anisotropic. To numerically solve the anisotropic dispersion, negative concentrations induced by artificial oscillations will appear, no matter which numerical method is employed. Many methods have been proposed to solve this difficult problem. An improved mesh-free method was proposed by Herrera et al. [28] to simulate conserved solute transport in heterogeneous layers under various Peclet numbers. A new approximation for anisotropic dispersion of SPH was then derived by Herrera et al. [29]. To reduce the non-physical oscillation and negative concentration caused by the diffusion tensor, Avesani et al. [30] proposed an improved SPH method based on a moving-least-squares-weighted-essentially non-oscillatory (MLS-WENO) scheme. Tran-Duc et al. [31] proposed a new SPH method and verified its accuracy through typical anisotropic examples. Recently, the anisotropic dispersion of solute in porous media was simulated by Alvarado-Rodriguez et al. [32] using the consistent SPH method. Even though increasing the number of particles within the neighborhood could ensure convergence, negative concentrations still presented and tremendous computational time was needed when the smoothing length became large [33].

Particle inconsistency is a longstanding shortcoming of the standard SPH method. The lack of integrability of particle approximation (i.e., spatial discretization of the kernel approximation) is one of the main reasons. This inevitably results in a loss of accuracy. Therefore, another focus of solving the ADE with SPH is to restore particle consistency. Many scholars have investigated this issue. For example, Li and Liu [34] and Liu et al. [35] proposed relatively simple methods for restoring consistency by modifying the function, thus ensuring that the polynomial is accurately interpolated into the calculation process. Bonet and Lok [36] proposed a gradient correction method based on the variational formula of SPH, which accurately evaluates the gradient of a linear function. The truncation error of spatial derivative approximation and its influencing factors were analyzed by Quinlan et al. [37]. A more stable method of restoring consistency is to use the Taylor series expansion of the basic kernel function and its derivatives. Based on this idea, Chen et al. [24,38] proposed the corrective smoothed particle method (CSPM), which subsequently approximates the kernel function and its first derivatives by ignoring the higher-order derivative terms in the Taylor series expansion. By retaining only the function and its first-order derivative in the Taylor series expansion, the finite particle method (FPM) is presented by Liu and Liu [39], in which the coupled linear equations are solved simultaneously. The FPM scheme was subsequently improved by Zhang and Batra [40], who retained derivatives up to second order in the Taylor series expansion. Further improvements have since been made to the modified SPH (MSPH) method [40] to obtain symmetric SPH (SSPH) [41]. The methods based on Taylor series expansion are very effective in restoring particle consistency. However, when higher-order derivatives are retained, the number of algebraic linear equations to be solved increases rapidly, whereby the computational efficiency quickly drops. A new strategy was proposed in which the number of neighbor particles in the support domain was dynamically increased with the increasing smoothing length [32,42], but this approach is computationally expensive. Recently, Sigalotti et al. [43] derived new consistency integral relations for particle approximation by theoretical analysis.

Non-physical oscillations occur in the DF format [15], but the conditions and causes that lead to these oscillations are not clear. To solve this problem, they are theoretically analyzed and numerically examined in this paper. By analyzing different oscillation conditions, a new partial diffusive flux (PDF) format is further proposed. Different from previous methods [44,45], which require complex judgments according to different conditions to avoid oscillations, the PDF format fundamentally avoids the numerical deficiency of non-physical oscillations. Moreover, to restore particle consistency while balancing computational accuracy and efficiency, the CSPM is used to compute all partial derivatives. To verify the capabilities of the proposed method, theoretical analysis is applied to demonstrate its stability, and one- and two-dimensional advection–diffusion problems with initial discontinuities are tested numerically.

The remainder of this paper is organized as follows. Section 2 presents the SPH method in DF format. The conditions and causes leading to non-physical oscillations are analyzed in Section 3. In Section 4, the improved SPH method in PDF format is presented. The DF and PDF formats are then tested in Section 5 by considering five typical cases. Finally, the conclusions are given in Section 6.

2. SPH method in DF format

Any given function $f(x)$ can be written in the following integral form [7] as:

$$f(x) = \int_{\Omega} f(x')\delta(x - x')dx', \tag{3}$$

where Ω is the problem domain and $\delta(x - x')$ is the Dirac function, defined as:

$$\delta(x - x') = \begin{cases} 1 & x = x', \\ 0 & x \neq x'. \end{cases} \tag{4}$$

Considering the ideal properties of the Dirac function, a kernel function $W(x - x', h)$ is introduced to approximate it. Equation (3) then becomes:

$$\langle f(x) \rangle = \int_{\Omega} f(x')W(x - x', h)dx', \tag{5}$$

where $\langle f(x) \rangle$ represents the kernel approximation of the function and h is the smoothing length of the kernel. There are several rules governing the properties and selection of the kernel function [46]. The most extensively used B-spline function is adopted in this paper [47].

In SPH, the problem domain is discretized into a set of particles and the integral function in Eq. (5) is then further approximated by a discrete summation:

$$\langle f(x_i)\rangle = \sum_{j=1}^{N} f(x_j) W(x_i - x_j, h) \triangle V_j, \tag{6}$$

where $\triangle V_j$ is the volume of particle j.

The derivative of Eq. (6) can be obtained as:

$$\langle \nabla f(x_i)\rangle = \sum_{j=1}^{N} f(x_j) \nabla_i W_{ij} \triangle V_j, \tag{7}$$

where $\nabla_i W_{ij} = \partial W(|x_i - x_j|, h_i)/\partial x_i$. As the derivative of the kernel is antisymmetric, we have:

$$\int_{\Omega} \nabla W(x - x', h) dx' = 0. \tag{8}$$

The most widely used spatial derivative approximation can then be obtained as:

$$\langle \nabla f_i\rangle = \sum_{j=1}^{N} \left(f_j - f_i\right) \nabla_i W_{ij} \triangle V_j, \tag{9}$$

where $f_i = f(x_i)$. Similarly, the second derivative of the function at particle i can be approximated as:

$$\langle \nabla(\nabla f_i)\rangle = \sum_{j=1}^{N} \left(\left\langle \nabla f_j \right\rangle - \langle \nabla f_i\rangle\right) \nabla_i W_{ij} \triangle V_j. \tag{10}$$

3. DF format oscillations analysis

In this section, the reason for the non-physical oscillations at discontinuities that occur in the DF format is analyzed, and the cases likely to cause oscillations are inferred. Note that SPH-DF is used hereafter to represent the SPH method in DF format. To analyze the causes of non-physical oscillations, the following one-dimensional pure diffusion equation is considered:

$$\frac{\partial u}{\partial t} = \frac{\partial}{\partial x}\left(D \frac{\partial u}{\partial x}\right). \tag{11}$$

3.1. Discontinuity analysis

Without losing generality, the diffusion coefficient D is taken as unity here. Assuming equal particle spacing, the initial condition for u can be considered as u_i for x_i and the smoothing radius $h = n\Delta x$ is taken. Equation (9) can then be written as:

$$\begin{aligned}
\left\langle \frac{\partial u}{\partial x}\right\rangle_i &= \sum_{s=-m}^{m} (u_{i+s} - u_i) W'\left(\frac{s}{n}\right), \\
&= \sum_{s=1}^{m} (u_{i+s} - u_i) W'\left(\frac{s}{n}\right) + \sum_{s=-1}^{-m} (u_{i+s} - u_i) W'\left(\frac{s}{n}\right), \\
&= \sum_{s=1}^{m} (u_{i+s} - u_i) W'\left(\frac{s}{n}\right) + \sum_{s=1}^{m} (u_{i-s} - u_i) W'\left(\frac{-s}{n}\right), \\
&= \sum_{s=1}^{m} \left[(u_{i+s} - u_i) - (u_{i-s} - u_i)\right] W'\left(\frac{s}{n}\right), \\
&= \sum_{s=1}^{m} \left[u_{i+s} - u_{i-s}\right] W'\left(\frac{s}{n}\right),
\end{aligned} \tag{12}$$

where m represents the number of particles that can be searched on each side of particle i and $m = \lfloor 2n \rfloor$.

The second-order derivative in Eq. (10) reduces to:

$$\begin{aligned}
\left\langle \frac{\partial}{\partial x}\left(\frac{\partial u}{\partial x}\right)\right\rangle_i &= \sum_{k=1}^{m} \left[\left\langle \frac{\partial u}{\partial x}\right\rangle_{i+k} - \left\langle \frac{\partial u}{\partial x}\right\rangle_{i-k}\right] W'\left(\frac{k}{n}\right), \\
&= \sum_{k=1}^{m} \left[\sum_{s=1}^{m} \left[u_{i+s+k} - u_{i-s+k}\right] W'\left(\frac{s}{n}\right) - \sum_{s=1}^{m} \left[u_{i+s-k} - u_{i-s-k}\right] W'\left(\frac{s}{n}\right)\right] W'\left(\frac{k}{n}\right), \\
&= \sum_{k=1}^{m} \left[\sum_{s=1}^{m} \left[u_{i+s+k} - u_{i-s+k} - u_{i+s-k} + u_{i-s-k}\right] W'\left(\frac{s}{n}\right)\right] W'\left(\frac{k}{n}\right), \\
&= \sum_{k=1}^{m} \sum_{s=1}^{m} \left[u_{i+s+k} - u_{i-s+k} - u_{i+s-k} + u_{i-s-k}\right] W'\left(\frac{s}{n}\right) W'\left(\frac{k}{n}\right).
\end{aligned} \tag{13}$$

Table 1
Concentrations and second-order derivative values in SPH-DF for $n = 1.33$, where $a_1 = W'\left(\frac{1}{n}\right)W'\left(\frac{1}{n}\right), a_2 = 2W'\left(\frac{2}{n}\right)W'\left(\frac{1}{n}\right), a_3 = W'\left(\frac{2}{n}\right)W'\left(\frac{2}{n}\right)$.

x_i	-3	-2	-1	0	1	2	3	4
u_i	0	0	0	0	1	1	1	1
$\left\langle \frac{\partial^2 u}{\partial x^2} \right\rangle_i$	a_1	$a_1 + a_2$	$a_1 + a_2 + a_3$	$a_1 + a_3$	$-a_1 - a_3$	$-a_1 - a_2 - a_3$	$-a_1 - a_2$	$-a_1$

Table 2
Second-order derivative values in SPH-DF for $n = 1.33$ and $n = 1.51$, where $a_1 = W'\left(\frac{1}{n}\right)W'\left(\frac{1}{n}\right), a_2 = 2W'\left(\frac{2}{n}\right)W'\left(\frac{1}{n}\right), a_3 = W'\left(\frac{2}{n}\right)W'\left(\frac{2}{n}\right), a_4 = 2W'\left(\frac{3}{n}\right)W'\left(\frac{1}{n}\right), a_5 = 2W'\left(\frac{3}{n}\right)W'\left(\frac{2}{n}\right), a_6 = W'\left(\frac{3}{n}\right)W'\left(\frac{3}{n}\right)$.

$\left\langle \frac{\partial^2 u}{\partial x^2} \right\rangle_i$	-3	-2	-1	0	1	2	3	4
$n = 1.33$	a_1	$a_1 + a_2$	$a_1 + a_2 + a_3$	$a_1 + a_3$	$-a_1 - a_3$	$-a_1 - a_2 - a_3$	$-a_1 - a_2$	$-a_1$
$n = 1.51$	$a_3 + a_4 + a_5 + a_6$	$a_2 + a_3 + a_4 + a_5 + a_6$	$a_1 + a_2 + a_3 + a_5 + a_6$	$a_1 + a_3 + a_6$	$-a_1 - a_3 - a_6$	$-a_1 - a_2 - a_3 - a_5 - a_6$	$-a_2 - a_3 - a_4 - a_5 - a_6$	$-a_3 - a_4 - a_5 - a_6$

If the Euler method is applied for time marching, the time integral becomes:

$$u_i^{t+\triangle t} = u_i^t + \triangle t \left\langle \frac{\partial}{\partial x}\left(\frac{\partial u}{\partial x}\right)\right\rangle_{i,t}. \tag{14}$$

With a discontinuous initial condition, the concentrations and coefficients in the second derivative are as listed in Table 1 for $n = 1.33$ and $m = 2$. For $x_i = 0$, the second derivative is less than that for $x_i = -1$, and for $x_i = 1$, the second derivative is larger than that for $x_i = 2$. Both of these issues cause non-physical oscillations.

According to Eq. (13) and Table 1, the oscillations are caused by a missing term in the second derivative for particles at the discontinuity compared with adjacent ones. They occur independently of particle inconsistencies. As shown in Table 2, with the increasing smoothing radius, the number of missing terms increases, and thus the oscillations at the discontinuity will not disappear.

3.2. Non-physical oscillation condition

The cases that are likely to cause oscillations are now identified. Consider a more general case, where $u_{-3} = u_{-2} = 0$, $u_{-1} \geq 0$, $u_0 \gg u_{-1}$, $u_1 = u_2 = u_3 = u_4 \geq u_0$. This case has a monotonic increase in concentration and a rapid gradient change. To avoid non-physical oscillations, it is necessary to ensure that:

$$u_i^{t+\triangle t} \leq u_{i+1}^{t+\triangle t}. \tag{15}$$

Substituting Eqs. (13) and (14) into Eq. (15) yields:

$$2a_1(u_1 - u_0) + 2a_2(u_0 - u_{-1}) + 2a_3(u_1 - u_0) \leq \frac{u_1 - u_0}{\triangle t} + a_1 u_{-1}. \tag{16}$$

For the case shown in Table 1, we have $u_{-1} = 0$ and $u_0 = u_1$. Equation (16) is not satisfied, which means that non-physical oscillations will appear.

When $u_{-1} \neq 0$ and $u_1 = u_0$, Eq. (16) reduces to

$$\frac{u_0 - u_{-1}}{u_{-1}} \leq \frac{a_1}{2a_2}. \tag{17}$$

Since $u_{-2} = 0$, it can also be written as:

$$\frac{u_0 - u_{-1}}{u_{-1} - u_{-2}} \leq \frac{a_1}{2a_2}, \tag{18}$$

which means that the occurrence of oscillations is related to the change in gradient, regardless of the time step and the diffusion coefficient. Oscillations occur when the gradient changes significantly, which is referred to as the **Steep 1** condition. The lower limit of u_0 for which oscillations occur can be obtained by (18).

When $u_{-1} \ll u_0 < u_1$, Eq. (16) reduces to

$$2(a_1 + a_3) + 2a_2\frac{u_0 - u_{-1}}{u_1 - u_0} \leq \frac{1}{D\triangle t} + a_1\frac{u_{-1}}{u_1 - u_0}. \tag{19}$$

In this case, $u_0 - u_{-1} \gg u_1 - u_0$ leads to the possibility that Eq. (19) is not satisfied, depending on the time step and the diffusion coefficient. This is referred to as the **Steep 2** condition. Because $u_{-2} = 0$, Eq. (19) can also be written as:

$$2(a_1 + a_3) + 2a_2\frac{k_{-1}^+}{k_0^+} \leq \frac{1}{D\triangle t} + a_1\frac{k_{-1}^-}{k_0^+}, \tag{20}$$

where $k_0^+ = u_1 - u_0$, $k_0^- = k_{-1}^+ = u_0 - u_{-1}$, and $k_{-1}^- = u_{-1} - u_{-2}$. Here, k_i^+ and k_i^- are considered as the front and rear derivatives of x_i. The oscillations are induced by the correlation between the front and rear derivatives. When u_{-1} and u_0 are fixed, an upper bound of u_1 for which oscillations occur can be determined by (20).

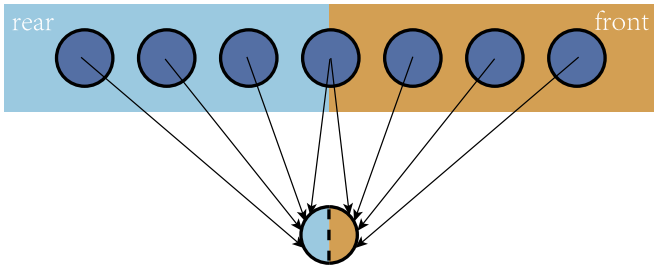

Fig. 1. Sketch of the first derivative approximation in SPH-PDF.

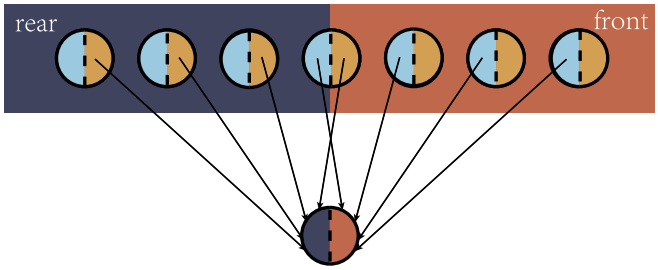

Fig. 2. Sketch of the second derivative approximation in SPH-PDF.

Remark 1. In the **Steep 2** condition, although oscillations can be avoided at the current time by reducing the time step $\triangle t$, the value of $\triangle t$ required will become smaller and smaller as u_1 gets closer to u_0. In this case, oscillations will eventually occur as the computation evolves.

4. SPH-PDF

Section 3 showed that the main factor affecting the oscillations in the SPH-DF format is the correlation between the front and rear derivatives. In this section, a new scheme is developed to calculate the flux by properly approximating the front and rear derivatives to avoid the oscillations.

4.1. Partial diffusive flux

Consider a scenario in which k_i^+ and k_i^- vary dramatically and the front and rear derivatives of particle i are different. As shown in Fig. 1, the points before x_i are selected to approximate the front derivative, and those behind x_i are selected to approximate the rear derivative.

First, the following indicative functions $I_{x^+}(j)$ and $I_{x^-}(j)$ are defined:

$$I_{x^+}(j) = \begin{cases} 1 & x_j \geq x_i, \\ 0 & x_j < x_i. \end{cases} \tag{21}$$

$$I_{x^-}(j) = \begin{cases} 1 & x_j \leq x_i, \\ 0 & x_j > x_i. \end{cases} \tag{22}$$

Equation (9) can then be written as:

$$\left\langle \frac{\partial u}{\partial x} \right\rangle_i^+ = \sum_{j \in \{x_j \geq x_i\}} (u_j - u_i) \nabla_i \hat{W}_{ij} \triangle V_j = \sum_{j=1}^{n} I_{x^+}(u_j - u_i) \nabla_i \hat{W}_{ij} \triangle V_j, \tag{23}$$

$$\left\langle \frac{\partial u}{\partial x} \right\rangle_i^- = \sum_{j \in \{x_j \leq x_i\}} (u_j - u_i) \nabla_i \hat{W}_{ij} \triangle V_j = \sum_{j=1}^{n} I_{x^-}(u_j - u_i) \nabla_i \hat{W}_{ij} \triangle V_j, \tag{24}$$

where $\hat{W}$ is a kernel function that approximates the flux using partial particles, as in the CSPM, MSPH, and SSPH. In the proposed method, the CSPM is used due to its simplicity and efficiency. As this new scheme uses partial particles, it is named as SPH-PDF.

Compared with the approximation of the flux, the calculation of the second-order derivatives $\left\langle \frac{\partial}{\partial x} \left(\frac{\partial u}{\partial x} \right) \right\rangle_i^+$ and $\left\langle \frac{\partial}{\partial x} \left(\frac{\partial u}{\partial x} \right) \right\rangle_i^-$ is not so intuitive. As shown in Fig. 2, the particles involved are the same as those used for the front and rear derivatives. However, for the front particles, the fluxes used for the second-order derivatives are those that point toward the central particle (their rear flux), while for the rear particles, the forward fluxes are used. In this case, Eq. (10) changes to:

$$\left\langle \frac{\partial}{\partial x} \left(\frac{\partial u}{\partial x} \right) \right\rangle_i^+ = \sum_{j=1}^{n} I_{x^+} \left(\left\langle \frac{\partial u}{\partial x} \right\rangle_j^- - \left\langle \frac{\partial u}{\partial x} \right\rangle_i^- \right) \nabla_i \hat{W}_{ij} \triangle V_j, \tag{25}$$

$$\left\langle \frac{\partial}{\partial x} \left(\frac{\partial u}{\partial x} \right) \right\rangle_i^- = \sum_{j=1}^{n} I_{x^-} \left(\left\langle \frac{\partial u}{\partial x} \right\rangle_j^+ - \left\langle \frac{\partial u}{\partial x} \right\rangle_i^+ \right) \nabla_i \hat{W}_{ij} \triangle V_j, \tag{26}$$

Table 3
Concentration and second-order derivative values in SPH-PDF for $n = 1.33$, where $a_1 = W'\left(\frac{1}{n}\right)\hat{W}'\left(\frac{1}{n}\right), a_2 = 2W'\left(\frac{2}{n}\right)\hat{W}'\left(\frac{1}{n}\right), a_3 = W'\left(\frac{2}{n}\right)\hat{W}'\left(\frac{2}{n}\right)$.

x_i	-3	-2	-1	0	1	2	3	4
u_i	0	0	0	0	1	1	1	1
$\left\langle \frac{\partial^2 u}{\partial x^2} \right\rangle_i^+$	0	0	a_2+a_3	$a_1+a_2+a_3$	$-a_1-a_2-a_3$	$-a_2-a_3$	0	0
$\left\langle \frac{\partial^2 u}{\partial x^2} \right\rangle_i^-$	0	0	a_2+a_3	$a_1+a_2+a_3$	$-a_1-a_2-a_3$	$-a_2-a_3$	0	0

$$\left\langle \frac{\partial}{\partial x}\left(\frac{\partial u}{\partial x}\right)\right\rangle_i = \frac{\left\langle \frac{\partial}{\partial x}\left(\frac{\partial u}{\partial x}\right)\right\rangle_i^+ + \left\langle \frac{\partial}{\partial x}\left(\frac{\partial u}{\partial x}\right)\right\rangle_i^-}{2}. \tag{27}$$

In the case of uniform particle distribution, the problems induced by discontinuities and the relationship between the front and rear second-order derivatives are analyzed in the next section.

4.2. SPH-PDF without oscillation

In this section, the proof that the SPH-PDF does not create oscillations at the discontinuities is provided and the rationality of Eq. (27) is explained.

4.2.1. Discontinuity analysis

Under the same conditions as in Section 3.1, Eq. (23) reduces to:

$$\left\langle \frac{\partial u}{\partial x}\right\rangle_i^+ = \sum_{s=1}^{m}(u_{i+s}-u_i)\hat{W}'\left(\frac{s}{n}\right), \tag{28}$$

and Eq. (24) reduces to:

$$\left\langle \frac{\partial u}{\partial x}\right\rangle_i^- = \sum_{s=1}^{m}(u_i-u_{i-s})\hat{W}'\left(\frac{s}{n}\right). \tag{29}$$

With Eqs. (28) and (29), the second-order derivative in Eq. (25) changes into:

$$\begin{aligned}
\left\langle \frac{\partial}{\partial x}\left(\frac{\partial u}{\partial x}\right)\right\rangle_i^+ &= \sum_{k=1}^{m}\left[\left\langle \frac{\partial u}{\partial x}\right\rangle_{i+k}^- - \left\langle \frac{\partial u}{\partial x}\right\rangle_i^-\right]\hat{W}'\left(\frac{k}{n}\right),\\
&= \sum_{k=1}^{m}\left[\sum_{s=1}^{m}\left[u_{i+k}-u_{i+k-s}\right]\hat{W}'\left(\frac{s}{n}\right) - \sum_{s=1}^{m}\left[u_i-u_{i-s}\right]\hat{W}'\left(\frac{s}{n}\right)\right]\hat{W}'\left(\frac{k}{n}\right),\\
&= \sum_{k=1}^{m}\left[\sum_{s=1}^{m}\left[u_{i+k}-u_{i+k-s}-u_i+u_{i-s}\right]\hat{W}'\left(\frac{s}{n}\right)\right]\hat{W}'\left(\frac{k}{n}\right),\\
&= \sum_{k=1}^{m}\sum_{s=1}^{m}\left[u_{i+k}-u_{i+k-s}-u_i+u_{i-s}\right]\hat{W}'\left(\frac{s}{n}\right)\hat{W}'\left(\frac{k}{n}\right),
\end{aligned} \tag{30}$$

and Eq. (26) becomes:

$$\begin{aligned}
\left\langle \frac{\partial}{\partial x}\left(\frac{\partial u}{\partial x}\right)\right\rangle_i^- &= \sum_{k=1}^{m}\left[\left\langle \frac{\partial u}{\partial x}\right\rangle_i^+ - \left\langle \frac{\partial u}{\partial x}\right\rangle_{i-k}^+\right]\hat{W}'\left(\frac{k}{n}\right),\\
&= \sum_{k=1}^{m}\left[\sum_{s=1}^{m}\left[u_{i+s}-u_i\right]\hat{W}'\left(\frac{s}{n}\right) - \sum_{k=1}^{m}\left[u_{i-k+s}-u_{i-k}\right]\hat{W}'\left(\frac{s}{n}\right)\right]\hat{W}'\left(\frac{k}{n}\right),\\
&= \sum_{k=1}^{m}\left[\sum_{s=1}^{m}\left[u_{i+s}-u_i-u_{i-k+s}+u_{i-k}\right]\hat{W}'\left(\frac{s}{n}\right)\right]\hat{W}'\left(\frac{k}{n}\right),\\
&= \sum_{k=1}^{m}\sum_{s=1}^{m}\left[u_{i+s}-u_i-u_{i-k+s}+u_{i-k}\right]\hat{W}'\left(\frac{s}{n}\right)\hat{W}'\left(\frac{k}{n}\right).
\end{aligned} \tag{31}$$

We can use Eq. (27) to rewrite the time integral in Eq. (14) as:

$$u_i^{t+\triangle t} = u_i^t + \frac{\triangle t}{2}\left(\left\langle \frac{\partial}{\partial x}\left(\frac{\partial u}{\partial x}\right)\right\rangle_{i,t}^+ + \left\langle \frac{\partial}{\partial x}\left(\frac{\partial u}{\partial x}\right)\right\rangle_{i,t}^-\right). \tag{32}$$

With the same discontinuous initial as that shown in Section 3.2, the values of the concentration and second-order derivatives are listed in Table 3 for $n = 1.33$ and $m = 2$. For $x_i = 0$, the second-order derivative is greater than that for $x_i = -1$, and for $x_i = 1$, it is less than that for $x_i = 2$. The method proposed in this paper fits the first- and second-order derivatives well at each point at discontinuities. Hence, the non-physical oscillations are avoided.

4.2.2. Relationship between front and rear second-order derivatives

Under the uniform particle distribution condition and using the same smoothing radii for the two "flux" calculations, the front and rear second-order derivatives are equal as indicated by

$$\begin{aligned}\left\langle \frac{\partial}{\partial x}\left(\frac{\partial u}{\partial x}\right)\right\rangle_i^+ &= \sum_{k=1}^{m}\sum_{s=1}^{m}\left[u_{i+k}-u_{i+k-s}-u_i+u_{i-s}\right]\hat{W}'\left(\frac{s}{n}\right)\hat{W}'\left(\frac{k}{n}\right),\\ &= \sum_{s=1}^{m}\sum_{k=1}^{m}\left[u_{i+k}-u_{i+k-s}-u_i+u_{i-s}\right]\hat{W}'\left(\frac{k}{n}\right)\hat{W}'\left(\frac{s}{n}\right),\\ &= \sum_{k=1}^{m}\sum_{s=1}^{m}\left[u_{i+s}-u_i-u_{i-k+s}+u_{i-k}\right]\hat{W}'\left(\frac{s}{n}\right)\hat{W}'\left(\frac{k}{n}\right),\\ &= \sum_{k=1}^{m}\sum_{s=1}^{m}\left[u_{i+s}-u_{i+s-t}-u_i+u_{i-k}\right]\hat{W}'\left(\frac{s}{n}\right)\hat{W}'\left(\frac{k}{n}\right) = \left\langle \frac{\partial}{\partial x}\left(\frac{\partial u}{\partial x}\right)\right\rangle_i^- .\end{aligned} \tag{33}$$

Hence the order of the two summations can be changed.

Note that when the particle distribution is not uniform, if the difference between the front and rear second-order derivatives is small, Eq. (27) is still rational.

4.3. Extension to high dimensions

In this subsection, the SPH-PDF is extended to the high dimensional cases. For two dimension, the following indicative functions $\mathbf{I}^+(j)$ and $\mathbf{I}^-(j)$ are defined as:

$$\mathbf{I}^+(j) = \begin{bmatrix} I_{x^+}(j) \\ I_{y^+}(j) \end{bmatrix}, \tag{34}$$

$$\mathbf{I}^-(j) = \begin{bmatrix} I_{x^-}(j) \\ I_{y^-}(j) \end{bmatrix}. \tag{35}$$

Then, Eq. (9) becomes:

$$\mathbf{q}_i^+ = \mathbf{D}_i \sum_j^n (u_j - u_i)\nabla_i \hat{W}_{ij} \circ \mathbf{I}^+(j) \tag{36}$$

$$\mathbf{q}_i^- = \mathbf{D}_i \sum_j^n (u_j - u_i)\nabla_i \hat{W}_{ij} \circ \mathbf{I}^-(j) \tag{37}$$

and Eq. (10) can be written as:

$$\mathbf{DF}_i^+ = \sum_j^n (\mathbf{q}_j^+ - \mathbf{q}_i^+)\circ\nabla_i \hat{W}_{ij} \circ \mathbf{I}^-(j), \tag{38}$$

$$\mathbf{DF}_i^- = \sum_j^n (\mathbf{q}_j^- - \mathbf{q}_i^-)\circ\nabla_i \hat{W}_{ij} \circ \mathbf{I}^+(j), \tag{39}$$

$$\mathbf{DF}_i = \frac{\mathbf{DF}_i^+ + \mathbf{DF}_i^-}{2}, \tag{40}$$

where $(\circ)$ represents the Hadamard product, i.e., element-wise product.

By adding an extra element for the third dimension in the indicative functions, extension of the SPH-PDF to the three-dimensional case is straightforward.

5. Numerical results and discussion

In this section, four typical ADE examples with the steep and discontinuous profiles are tested and the results of SPH in DF and PDF formats are compared with the exact solutions. For fair comparison, the CSPM is also used in SPH-DF as in SPH-PDF. The used error measure is the following L_2-norm error:

$$L_2 = \frac{\left[\sum_{i=1}^{N}\left(C_i^a - C_i^n\right)^2\right]^{\frac{1}{2}}}{\left[\sum_{i=1}^{N}\left(C_i^a\right)^2\right]^{\frac{1}{2}}}, \tag{41}$$

where C_i^a is the exact solution and C_i^n is the numerical solution. The numerical experiments are run on such hardware configurations: AMD Ryzen 7 7735H 3.20 GHz CPU with 16 GB of RAM.

5.1. Non-physical oscillation analysis

In this case, the theoretical proof presented in Section 3.2 is numerically verified. The conditions for the non-physical oscillations appeared in SPH-DF are presented and compared.

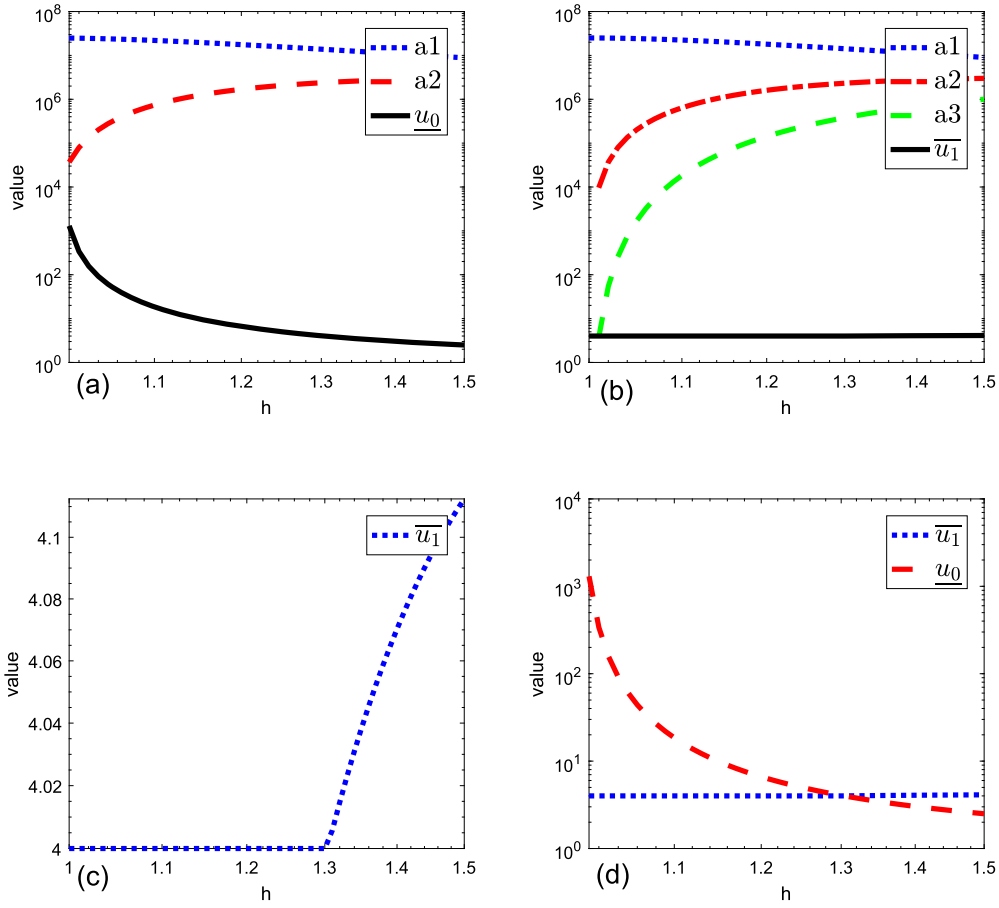

Fig. 3. Non-physical oscillation condition in different cases. (a) When $u_{-1} = 1$ and $u_1 = u_0$, lower limit of the oscillation of u_0 ($\underline{u_0}$), a_1, and a_2 under different h. (b) When $u_{-1} = 1$ and $u_0 = 4$, upper limit of the oscillation of u_1 ($\overline{u_1}$), a_1, a_2, and a_3 under different h. (c) $\overline{u_1}$ under different h. (d) Comparison of $\underline{u_0}$ and $\overline{u_1}$ under different h.

Table 4
Lower limit of u_0 ($\underline{u_0}$) for different h when $u_{-1} = 1$ and $u_1 = u_0$.

Variable	Value					
h	1.1	1.2	1.3	1.33	1.4	1.5
$\underline{u_0}$	18.500	6.625	4.056	3.663	3.031	2.500

5.1.1. Analysis of first-time-step oscillation

We first consider the **Steep 1** condition for the case $u_{-1} = 1$ and $u_1 = u_0$. Fig. 3(a) compares a_1, a_2, and the lower limit of u_0 (i.e., $\underline{u_0}$). Oscillations only occur when u_0 is greater than $\underline{u_0}$. As the smoothing length h increases, $\underline{u_0}$ decreases. That is, larger values of h make oscillations more likely occur.

We now consider the **Steep 2** condition for the case $u_{-1} = 1$ and $u_0 = 4$. Fig. 3(b) compares a_1, a_2, a_3, and the upper limit of u_1 (i.e., $\overline{u_1}$). As shown in Fig. 3(c), non-physical oscillations occur when $h > 1.3$. As h increases, $\overline{u_1}$ increases. That is, larger values of h again make oscillations more likely occur.

In this case, the oscillations with $h > 1.3$ in the **Steep 2** condition can be explained by comparing the values of u_0 and $\overline{u_1}$ shown in Fig. 3(d). When $h < 1.3$, u_0 (dashed line) is greater than $\overline{u_1}$ (dotted line), indicating that Eq. (18) holds even when $u_1 = u_0$, and so oscillations are avoided. When $h > 1.3$, $\underline{u_0}$ is less than $\overline{u_1}$, so Eq. (19) must be satisfied to avoid the oscillations.

Remark 2. Different values of u_0 result in different intersection points between $\overline{u_1}$ and $\underline{u_0}$.

The values of $\underline{u_0}$ and $\overline{u_1}$ for typical values of h are presented in Tables 4 and 5. We see that $\underline{u_0}$ decreases rapidly as h increases, and $\overline{u_1}$ begins to increase when $h > 1.3$. When $h = 1.33$, we have $\overline{u_1} = 4.023$ (see Table 5), which implies that the first-time-step oscillation can be avoided if $u_1 > 4.023$ holds in the **Steep 2** condition. However, according to Remark 1, the oscillations cannot be fully prevented for $u_1 > 4.023$. Some specific experiments are presented below.

Table 5
Upper bound of u_1 ($\overline{u_1}$) for different h when $u_{-1} = 1$ and $u_0 = 4$.

Variable	Value					
h	1.1	1.2	1.3	1.33	1.4	1.5
$\overline{u_1}$	——	——	——	4.023	4.070	4.112

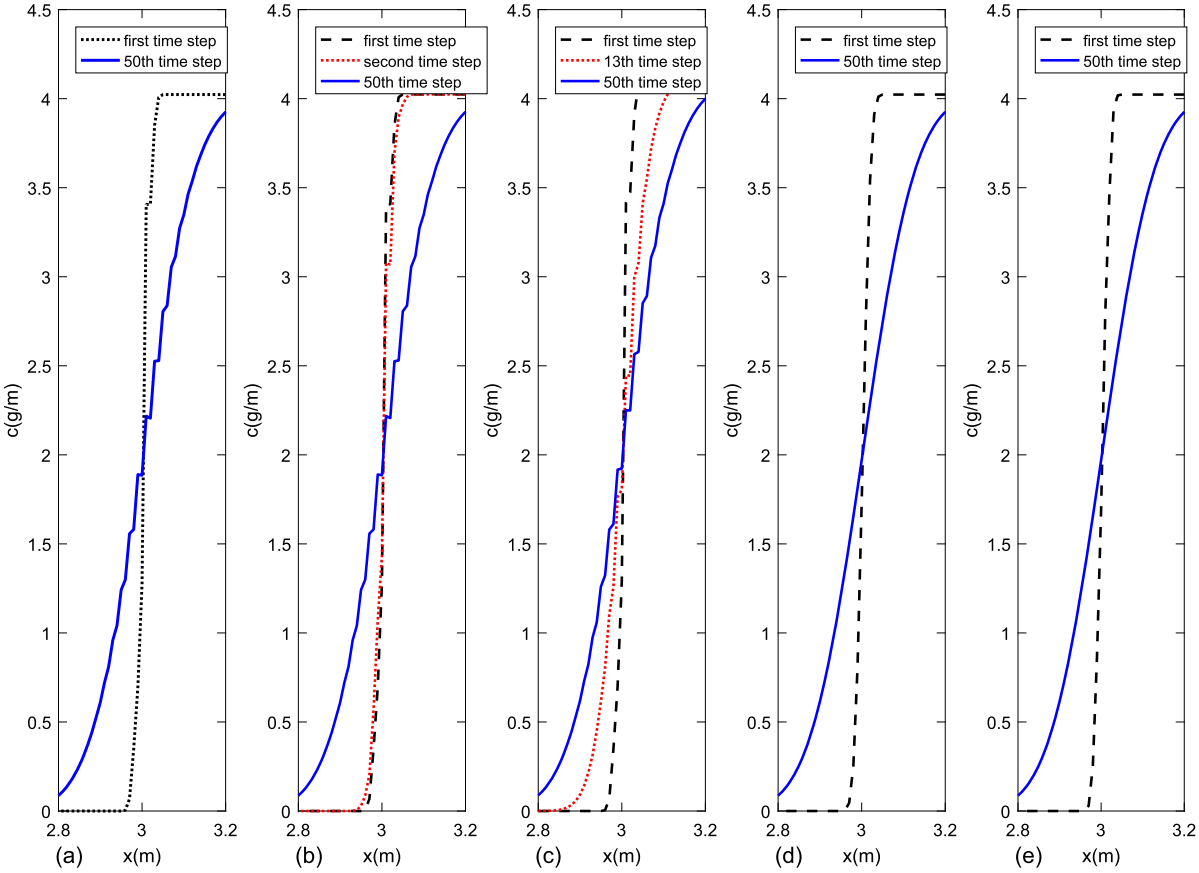

Fig. 4. Numerical oscillations of SPH-DF comparing with SPH-PDF and method in Ref. [32]. (a) When $u_1 = 4.023$, the oscillation appears at the first time step, (b) when $u_1 = 4.024$, the oscillation appears at the second time step, and (c) when $u_1 = 4.1$, oscillations appear at the 13th time step. When $u_1 = 4.023$, the oscillation disappears in (d) SPH-PDF and (e) the method in Ref. [32].

5.1.2. Illustration of non-physical oscillations

This section presents three examples to illustrate the **Steep 2** condition of oscillations. The governing equation for these three examples is:

$$\frac{\partial c}{\partial t} = \frac{\partial}{\partial x}\left(D\frac{\partial c}{\partial x}\right), x \in [0,6], t \in [0,0.5], \tag{42}$$

with the following initial and boundary conditions:

$$\begin{cases} c(x,0) = 0, & 0 \le x < 3 \\ c(x,0) = 1, & x = 3 \\ c(x,0) = 4, & x = 3.01 \\ c(x,0) = u_1, & otherwise \end{cases}, \quad c(0,t) = 0, \quad c(1,t) = u_1. \tag{43}$$

The following parameters are considered in this test: $D = 0.01$, $\triangle t = 0.01$, and $\triangle x = 0.01$.

Fig. 4 compares the three cases with different u_1 values. When $u_1 = 4.023$, as shown in Table 5, non-physical oscillations occur at the first time step. Fig. 4(a) illustrates that an oscillation occurs at the first time step and the oscillations remain until the end time step. In Fig. 4(b), when $u_1 = 4.024$, there is no oscillation at the first time step, but an oscillation appears at the second step and persists in subsequent steps. In Fig. 4(c), when $u_1 = 4.1$, the oscillations appear at the 13th step and remain thereafter. In Fig. 4(d) and (e), even when $u_1 = 4.023$, the oscillation disappears in SPH-PDF and the method in Ref. [32].

As stated in Remark 1, as u_0 approaches u_1, $\triangle t$ must become smaller. Thus, even if no oscillations occur in the first few steps, the possibility of oscillations still exists in later steps.

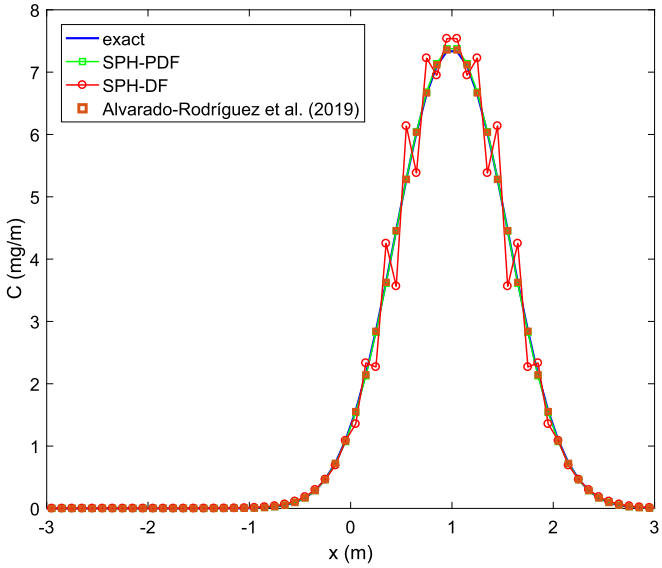

Fig. 5. Comparison of numerical results obtained by SPH-DF, SPH-PDF and Ref. [32] with the exact solution for the one-dimensional discontinuous problem.

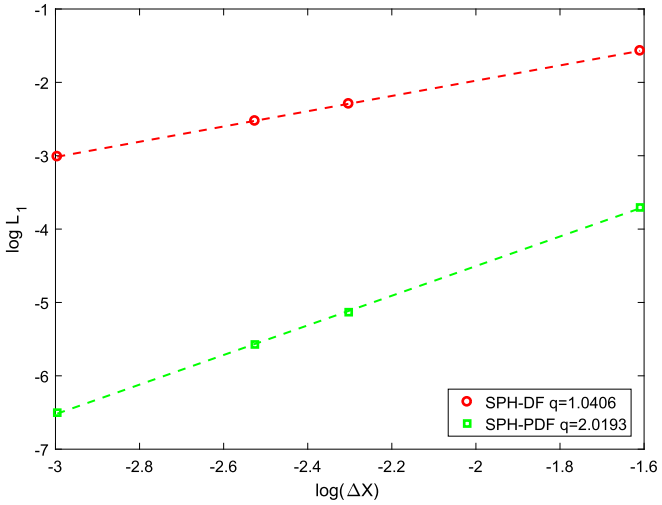

Fig. 6. Comparison of the convergence behavior of SPH-DF and SPH-PDF for the one-dimensional discontinuous problem.

5.2. One-dimensional discontinuous problem

In this case, a one-dimensional discontinuous advection–diffusion problem is considered. The governing equation is:

$$\frac{\partial c}{\partial t}+v\frac{\partial c}{\partial x}=\frac{\partial}{\partial x}\left(D\frac{\partial c}{\partial x}\right), x\in[-3,3], t\in[0,1], \tag{44}$$

with the initial and boundary conditions:

$$\begin{cases} c(x,0)=C_0, & x_1\le x<x_2 \\ c(x,0)=0, & otherwise \end{cases}, c(-3,t)=0, c(3,t)=0. \tag{45}$$

The exact solution is:

$$c(x,t)=\frac{C_0}{2}\left[erf\left(\frac{x-x_1-vt}{\sqrt{4tD}}\right)-erf\left(\frac{x-x_2-vt}{\sqrt{4tD}}\right)\right]. \tag{46}$$

The following parameters are taken in this test: $D=0.1$, $v=1$, $C_0=10$, $x_1=-0.5$, and $x_2=0.5$.

The numerical results obtained by SPH-DF, SPH-PDF and the consistent SPH [32] are compared with the exact solution in Fig. 5. Excellent agreement between the solutions of SPH-PDF and the consistent SPH [32] and the exact result is clearly observed, while non-physical oscillations appear in the SPH-DF case. The fitted curves of the relationship between the natural logarithms of the numerical error and spatial step size are shown in Fig. 6. The convergence rate of SPH-DF is 1.0406, while that of SPH-PDF is 2.0193, which is the expected second-order rate. In addition, the numerical error of the SPH-PDF scheme is over two orders of magnitude smaller than that of SPH-DF. The computational times of SPH-DF and SPH-PDF with different particle numbers are compared in Table 6. No noticeable time increment is observed for the improved method.

Table 6
Computational time of two SPH methods with different particle numbers (s).

Particle number	20	40	50	60	80	100
SPH-DF	0.995	1.616	1.858	2.023	2.607	3.122
SPH-PDF	0.949	1.581	1.744	1.961	2.466	3.222

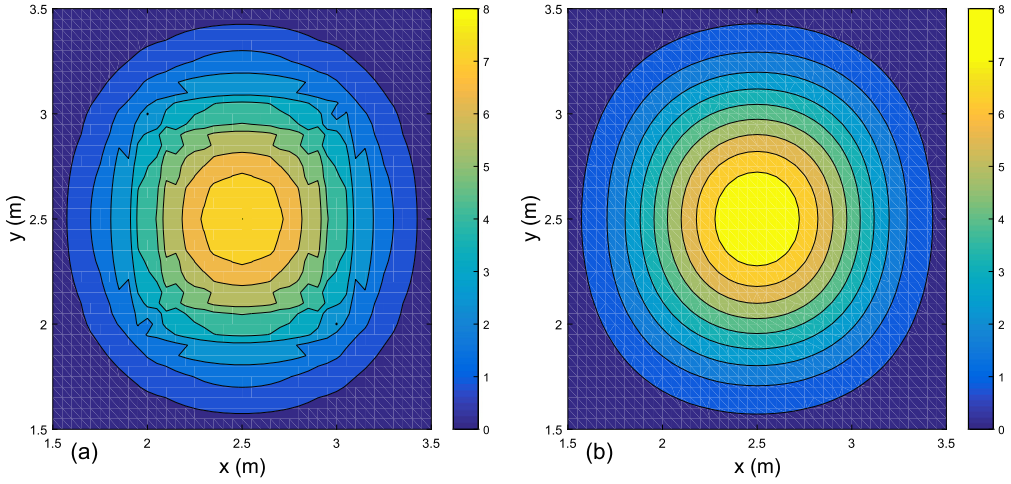

Fig. 7. Comparison of numerical results obtained by SPH-DF and SPH-PDF for the two-dimensional discontinuous problem.

5.3. Two-dimensional discontinuous problem

In this case, a two-dimensional discontinuous example is tested. The governing equation is:

$$\frac{\partial c}{\partial t}+u\frac{\partial c}{\partial x}+v\frac{\partial c}{\partial y}=\frac{\partial}{\partial x}\left(D\frac{\partial c}{\partial x}\right)+\frac{\partial}{\partial y}\left(D\frac{\partial c}{\partial y}\right), x\in[0,4], y\in[0,4], t\in[0,4], \tag{47}$$

and the initial-boundary conditions are:

$$\begin{cases} c(x,y,0)=C_0, & (x,y)\in[x_1,x_2]\times[y_1,y_2] \\ c(x,y,0)=0, & otherwise \end{cases}, \tag{48}$$

$$c(0,y,t)=0, c(4,y,t)=0, c(x,0,t)=0, c(x,4,t)=0. \tag{49}$$

The exact solution for this case is:

$$c(x,y,t)=\frac{C_0}{4}\left[erf\left(\frac{x-x_1-ut}{\sqrt{4tD}}\right)-erf\left(\frac{x-x_2-ut}{\sqrt{4tD}}\right)\right]*\left[erf\left(\frac{y-y_1-vt}{\sqrt{4tD}}\right)-erf\left(\frac{y-y_2-vt}{\sqrt{4tD}}\right)\right]. \tag{50}$$

The following parameters are considered in this test: $u=1$, $v=1$, $D=0.01$, $C_0=10$, $x_1=y_1=2$, and $x_2=y_2=3$.

Fig. 7 presents the concentration distribution contours for the results given by SPH-DF and SPH-PDF. Non-physical oscillations appear in a localized range for SPH-DF, and the specific areas of oscillation are indicated by concentration contours in the overall range. However, the concentration contours given by SPH-PDF are smooth and do not exhibit any oscillations.

The concentrations along the cross-section at $y=2.5$ and $t=5$ are shown in Fig. 8, together with the exact solution. Comparing the numerical results with the exact solution, the oscillations similar as those in the one-dimensional case are produced by SPH-DF, while the SPH-PDF generates no oscillations and its results are in excellent agreement with the exact solution.

The convergence behavior of the SPH-DF and SPH-PDF schemes for this two-dimensional case is also studied. The fitted curves of the relationship between the natural logarithms of the numerical error and spatial step size are shown in Fig. 9. Compared with the convergence rate of SPH-DF which is 1.067, SPH-PDF's is 2.186 and it is second-order again. In addition, the numerical error of the SPH-PDF scheme is at least one order of magnitude lower than that of SPH-DF.

5.4. Anisotropic dispersion case

In this case, a two-dimensional anisotropic example from Ref. [32] is tested. The governing equation is:

$$\frac{\partial c}{\partial t}+u\frac{\partial c}{\partial x}+v\frac{\partial c}{\partial y}=\nabla\cdot(\mathbb{D}\cdot\nabla c), \tag{51}$$

where $\mathbb{D}$ is the second-rank diffusion coefficient tensor. The initial condition is:

$$c(x,y,0)=C_0\exp\left[-\frac{(x-x_0)^2+(y-y_0)^2}{2\sigma^2}\right] \tag{52}$$

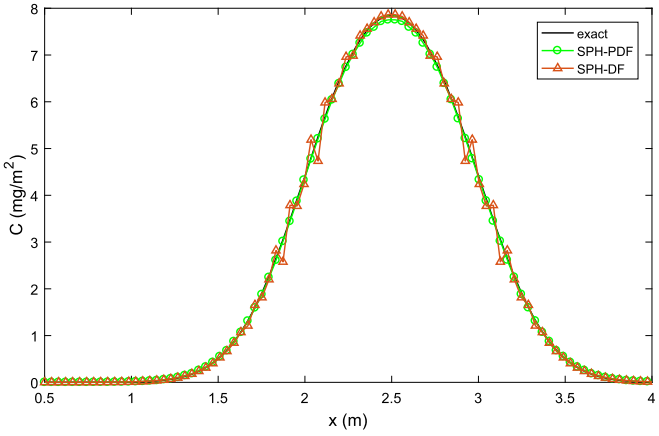

Fig. 8. Comparison of numerical results obtained by SPH-DF and SPH-PDF with the exact solution at the cross-section of $y = 2.5$ and $t = 5$ for the two-dimensional discontinuous problem.

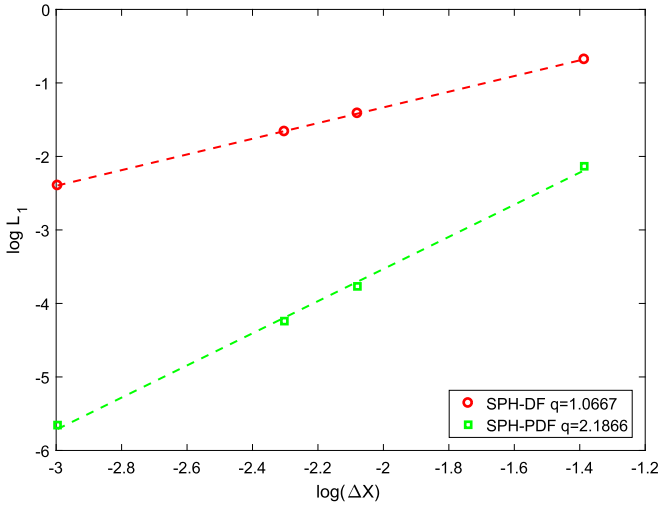

Fig. 9. Comparison of the convergence behavior of SPH-DF and SPH-PDF for the two-dimensional discontinuous problem.

The exact solution for this case is:

$$\frac{C(x,y,t)}{C_0} = \frac{w^2}{C_3} \exp\left[\frac{-\left(x-x_0-ut\right)^2 A_1 - \left(y-y_0-vt\right)^2 A_2 + 4\left(x-x_0-ut\right)\left(y-y_0-vt\right) A_3}{8t^2 C_2 + 4w^1 t C_2 + 2w^4}\right], \tag{53}$$

in which:

$$\begin{aligned} &A_1 = 2tD_{yy} + w^2 && A_2 = 2tD_{xx} + w^2 \quad A_3 = tD_{xy} \\ &C_1 = D_{xx}D_{yy} - D_{xy}^2 && C_2 = D_{xx} + D_{yy} \quad C_3 = \left(4t^2 C_1 + 2tw^2 C_2 + w^4\right)^{1/2} \\ &D_{ij} = (\alpha_T |\mathbf{V}| + D_m)\delta_{ij} + (\alpha_L - \alpha_T)\frac{uv}{|\mathbf{V}|} && |\mathbf{V}| = \sqrt{u^2 + v^2} \end{aligned} \tag{54}$$

where D_m is the molecular diffusion coefficient and δ_{ij} is the Kronecker delta. The following parameters are considered in this test: $u = v = 1$ m/s, $D_m = 0.0$, $\alpha_L = 10$, $\alpha_T/\alpha_L = 0.01$, $C_0 = 320$ mg/L, and $x_0 = y_0 = 1000$ m.

Fig. 10 presents the concentration distribution contours for the results obtained by SPH-DF, SPH-PDF and the consistent SPH [32]. Negative concentrations are observed in the solutions of three methods at -7.8203e-31, -1.1996e-07, and -2.9024e-05, respectively. Good results are obtained by SPH-DF and SPH-PDF. The negative concentration in SPH-PDF is two magnitudes lower than that of the consistent SPH [32]. Therefore, an encouraging possibility is provided for the application of the SPH with diffusive flux to the anisotropic dispersion.

5.5. One-dimensional Gaussian case

As the CSPM is used to calculate the first-order derivatives in the SPH-PDF scheme, the improved format is further compared with SPH-DF without CSPM and SPH-DF in this subsection. The governing equation for this case is:

$$\frac{\partial c}{\partial t} + v\frac{\partial c}{\partial x} = \frac{\partial}{\partial x}\left(D\frac{\partial c}{\partial x}\right), x \in [-3,3], t \in [0,1], \tag{55}$$

and the initial-boundary conditions are:

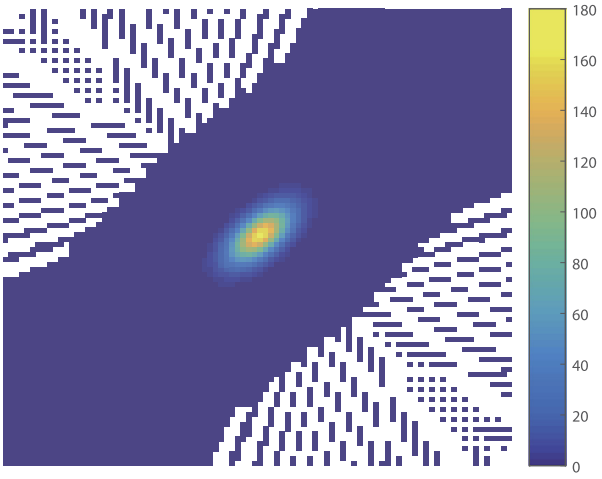

(a)

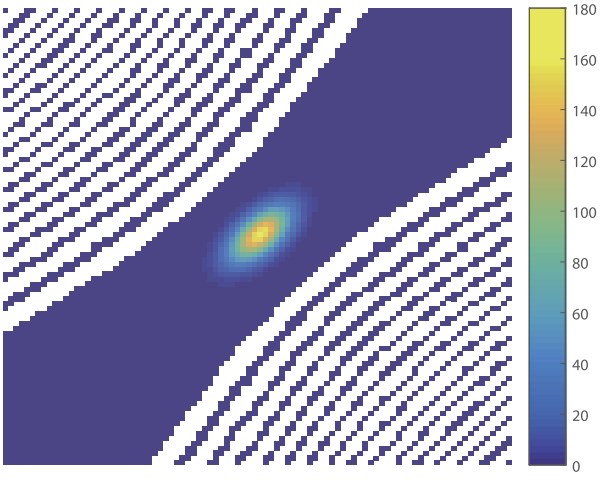

(b)

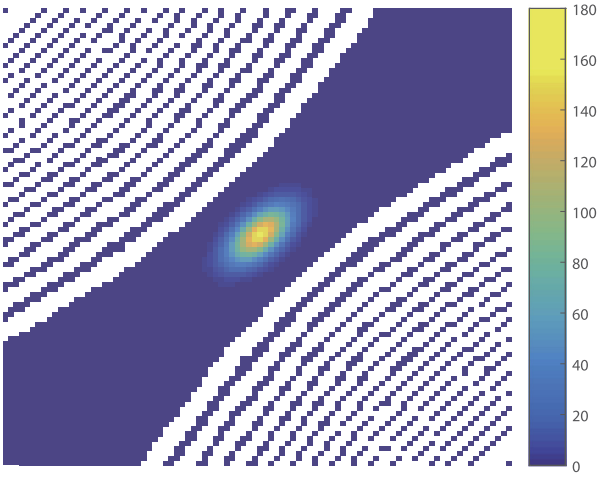

(c)

Fig. 10. Comparison of the convergence behavior of (a) SPH-DF, (b) SPH-PDF with (c) Ref. [32] for the two-dimensional anisotropic problem.

$$c(x,0) = \exp\left(-\frac{(x-\mu)^2}{2\sigma^2}\right), c(-3,t) = 0, c(3,t) = 0. \tag{56}$$

The exact solution for this case is:

$$c(x,t) = \frac{\sigma}{\sqrt{\sigma^2 + 2Dt}} \exp\left(-\frac{(x-\mu-vt)^2}{2\sigma^2 + 4Dt}\right). \tag{57}$$

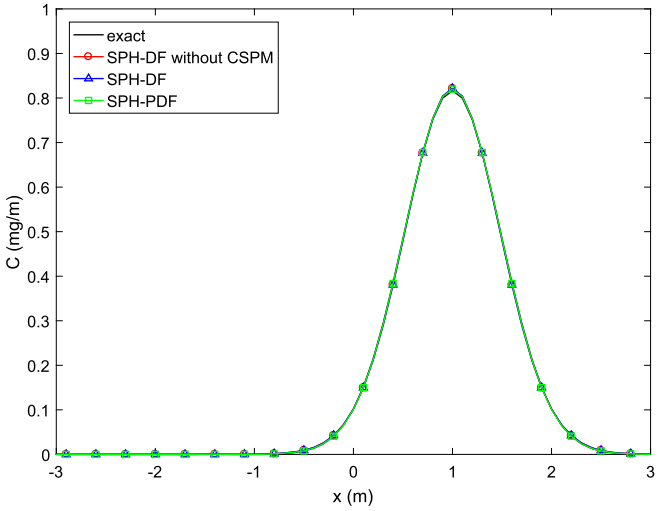

Fig. 11. Comparison of numerical results obtained by SPH-DF without CSPM, SPH-DF, and SPH-PDF with the exact solution in the one-dimensional Gaussian case.

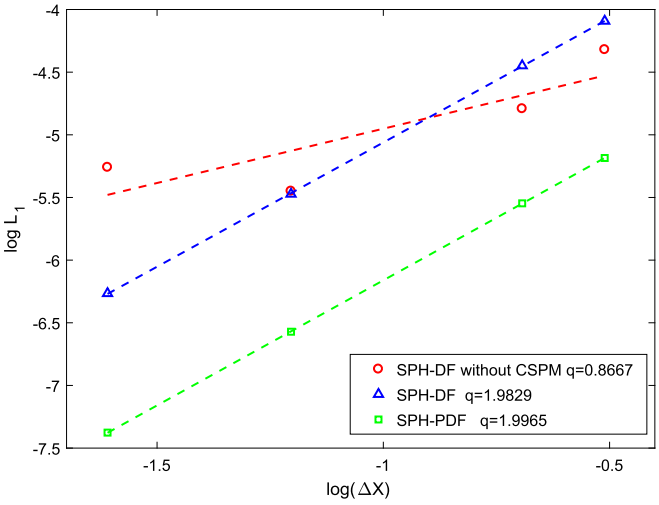

Fig. 12. Comparison of convergence behavior for SPH-DF without CSPM, SPH-DF, and SPH-PDF in the one-dimensional Gaussian case.

The following parameters are considered in this test: $D = 0.04$, $v = 2$, $\mu = -1$, and $\sigma = 0.1$.

Fig. 11 shows that the numerical results given by SPH-DF without CSPM, SPH-DF, and SPH-PDF are all correct and have good agreements with the exact solution. The fitted curves of the relationship between the natural logarithms of the numerical error and spatial step size are shown in Fig. 12. The convergence rate is 1.9829 for SPH-DF and 1.9965 for SPH-PDF, both of which are close to the expected second-order. The numerical error of the SPH-PDF scheme is one order of magnitude lower than that of SPH-DF. For SPH-DF without CSPM, however, the convergence rate is only 0.8667. As the particle spacing decreases, the slope tends toward zero and may even become negative.

With the paremeters $D = 0.01$, $v = 1$, $\mu = 0$, and $\sigma = 0.1$, the SPH-PDF is tested with irregular and regular particle distributions. Fig. 13 shows that the numerical results given by SPH-PDF with irregular and regular particle distributions are all correct and have good agreements with the exact solution. The fitted curves of the relationship between the natural logarithms of the numerical error and spatial step size are shown in Fig. 14. The convergence rate is 2.2358 for the irregular case and 2.2638 for the regular one, both of which are second-order as expected.

6. Conclusion

In this study, a Lagrangian method based on smooth particle hydrodynamics (SPH) with diffusive flux is proposed and analyzed to solve advection-diffusion problems with discontinuities. The diffusive flux (DF) method using double first-order derivative calculations to approximate the second-order derivatives has been used to solve the advection–diffusion equation (ADE), which is closer to the physical process. The causes and conditions of the non-physical oscillations that arise in discontinuous problems have been theoretically analyzed and numerically verified. Based on this, a new scheme using partial diffusive flux (PDF) format was proposed to avoid these oscillations. Furthermore, the corrective smoothed particle method (CSPM) was applied to partial derivative calculation to avoid particle inconsistency and enhance numerical convergence. The behavior of the improved scheme was analyzed by applying it to five typical advection–diffusion problems with moving steep fronts, which are difficult for traditional mesh-based methods. The conclusions are drawn as follows:

- In the DF format, there is a missing term in the second derivative of particles at the discontinuity compared with adjacent particles, which causes the non-physical oscillations.

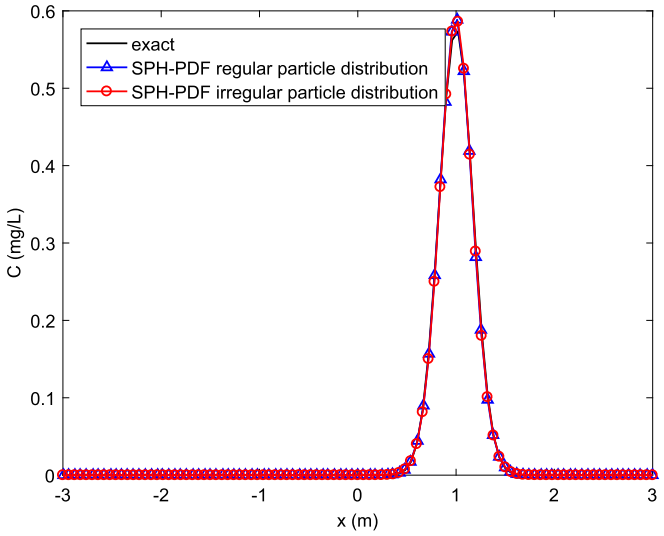

Fig. 13. Comparison of numerical results obtained by SPH-PDF with irregular and regular particle distributions with the exact solution in the one-dimensional Gaussian case.

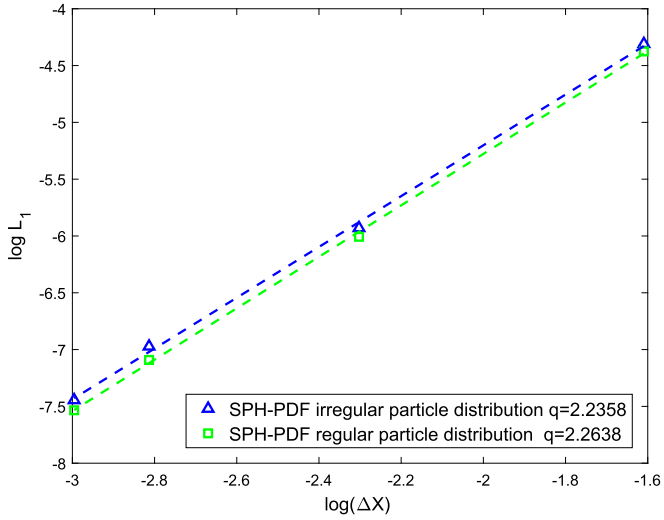

Fig. 14. Comparison of convergence behavior of SPH-PDF with irregular and regular particle distributions in the one-dimensional Gaussian case.

- The improved PDF format achieves second-order accuracy and second-order uniform convergence for advection–diffusion problems with discontinuities, and its error is at least one order of magnitude lower than that of the DF format.
- The second-order accuracy and uniform convergence are achieved for the proposed SPH-PDF format with both regular and irregular particle distributions.
- In the SPH-PDF format, using only partial particles leads to the appearance of particle inconsistencies, which can be avoided by using CSPM for first derivative approximations.

The application of the proposed smoothed particle hydrodynamics with diffusive flux to anisotropic dispersion has been conducted with promising results. More comprehensive studies and detailed comparisons with traditional SPH method are needed to fully explore the advantages of SPH-PDF. Furthermore, numerically solving the fluid dynamics problems using SPH requires the approximation of the second-order derivatives, e.g., the Laplacian in viscosity and pressure Poisson equation [48,49]. Therefore, how to properly formulate the Laplacian with diffusive flux will play a crucial role for the extension of SPH-PDF to fluid dynamics simulations.

Data availability

No data was used for the research described in the article.

Acknowledgements

This study was supported by the National Key Research and Development Program of China (Grant No. 2020YFC1807905), National Natural Science Foundation of China (Grant Nos. 52079090, U20A20316), and Basic Research Program of Qinghai Province (Grant No. 2022-ZJ-704).

References

[1] J. Zhang, H. Liu, A vertical 2-D numerical simulation of suspended sediment transport, J. Hydrodyn. 19 (2) (2007) 217–224.
[2] J.M. Restrepo, S.C. Venkataramani, C. Dawson, Nearshore sticky waters, Ocean Model. 80 (2014) 49–58.
[3] E.S. Gross, J.R. Koseff, S.G. Monismith, Evaluation of advective schemes for estuarine salinity simulations, J. Hydraul. Eng. 125 (1) (1999) 32–46.
[4] B.H. Devkota, J. Imberger, Lagrangian modeling of advection-diffusion transport in open channel flow, Water Resour. Res. 45 (12) (2009) W12406.
[5] J.J. Monaghan, Smoothed particle hydrodynamics, Rep. Prog. Phys. 68 (8) (2005) 1703–1759.
[6] T. Jiao, M. Ye, M. Jin, J. Yang, An interactively corrected smoothed particle hydrodynamics (IC-SPH) for simulating solute transport in a nonuniform velocity field, Water Resour. Res. 58 (6) (2022) e2021WR031017.
[7] R.A. Gingold, J.J. Monaghan, Smoothed particle hydrodynamics: theory and application to non-spherical stars, Mon. Not. R. Astron. Soc. 181 (3) (1977) 375–389.
[8] L.B. Lucy, Numerical approach to the testing of the fission hypothesis, Astron. J. 82 (12) (1977) 1013–1024.
[9] D. Violeau, B.D. Rogers, Smoothed particle hydrodynamics (SPH) for free-surface flows: past, present and future, J. Hydraul. Res. 54 (1) (2016) 1–26.
[10] H. Gotoh, A. Khayyer, On the state-of-the-art of particle methods for coastal and ocean engineering, Coast. Eng. J. 60 (1) (2018) 79–103.
[11] S.J. Lind, B.D. Rogers, P.K. Stansby, Review of smoothed particle hydrodynamics: towards converged Lagrangian flow modelling, Proc. R. Soc. A, Math. Phys. Eng. Sci. 476 (2241) (2020) 20190801.
[12] X. Bian, M. Ellero, A splitting integration scheme for the SPH simulation of concentrated particle suspensions, Comput. Phys. Commun. 185 (1) (2014) 53–62.
[13] Q. Hou, J. Liu, J. Lian, W. Lu, A Lagrangian particle algorithm (SPH) for an autocatalytic reaction model with multicomponent reactants, Processes 7 (7) (2019) 421.
[14] J. Ghazanfarian, R. Saghatchi, D. Patil, Implementation of smoothed particle hydrodynamics for non-linear Pennes' bioheat transfer equation, Appl. Math. Comput. 259 (2015) 21–31.
[15] R. Fatehi, M.A. Fayazbakhsh, M.T. Manzari, On discretization of second-order derivatives in smoothed particle hydrodynamics, World Acad. Sci., Eng. Technol. 40 (4) (2009) 243–246.
[16] E. Francomano, M. Paliaga, Highlighting numerical insights of an efficient SPH method, Appl. Math. Comput. 339 (2018) 899–915.
[17] Q. Hou, Z. Wang, J. Dang, W. Lu, Y. Cai, J. Wei, Simulation of heat conduction in fluids on GPU with particle method, Comput. Syst. Sci. Eng. 32 (2017) 481–489.
[18] L. Antonelli, E. Francomano, F. Gregoretti, A CUDA-based implementation of an improved SPH method on GPU, Appl. Math. Comput. 409 (2021) 125482.
[19] Y. Cai, J. Wei, Q. Hou, R. Gao, An optimized GPU implementation of weakly-compressible SPH using CUDA-based strategies, in: ICA3PP 2021: Algorithms and Architectures for Parallel Processing, vol. 1, 2022, pp. 354–369.
[20] Q. Hou, C. Miao, S. Chen, Z. Sun, A. Karemat, A Lagrangian particle model on GPU for contaminant transport in groundwater, Comput. Part. Mech. 10 (3) (2022) 587–601.
[21] R.R. Bruce, A. Klute, The measurement of soil moisture diffusivity, Soil Sci. Soc. Am. J. 20 (4) (1956) 458–462.
[22] W. Huang, L. Zheng, X. Zhan, Adaptive moving mesh methods for simulating one-dimensional groundwater problems with sharp moving fronts, Int. J. Numer. Methods Eng. 54 (11) (2002) 1579–1603.
[23] M. Chaudhary, M.K. Singh, Study of multispecies convection-dispersion transport equation with variable parameters, J. Hydrol. 591 (2020) 125562.
[24] J. Chen, J. Beraun, C.J. Jih, Completeness of corrective smoothed particle method for linear elastodynamics, Comput. Mech. 24 (4) (1999) 273–285.
[25] J.H. Jeong, M.S. Jhon, J.S. Halow, J. Van Osdol, Smoothed particle hydrodynamics: applications to heat conduction, Comput. Phys. Commun. 153 (1) (2003) 71–84.
[26] S.J. Watkins, A.S. Bhattal, N. Francis, J.A. Turner, A.P. Whitworth, A new prescription for viscosity in smoothed particle hydrodynamics, Astron. Astrophys. Suppl. Ser. 119 (1) (1996) 177–187.
[27] L. Bonaventura, R. Ferretti, Semi-Lagrangian methods for parabolic problems in divergence form, SIAM J. Sci. Comput. 36 (5) (2014) A2458–A2477.
[28] P.A. Herrera, M. Massabó, R.D. Beckie, A meshless method to simulate solute transport in heterogeneous porous media, Adv. Water Resour. 32 (3) (2009) 413–429.
[29] P.A. Herrera, R.D. Beckie, An assessment of particle methods for approximating anisotropic dispersion, Int. J. Numer. Methods Fluids 71 (5) (2013) 634–651.
[30] D. Avesani, P. Herrera, G. Chiogna, A. Bellin, M. Dumbser, Smooth particle hydrodynamics with nonlinear moving-least-squares weno reconstruction to model anisotropic dispersion in porous media, Adv. Water Resour. 80 (2015) 43–59.
[31] T. Tran-Duc, E. Bertevas, N. Phan-Thien, B.C. Khoo, Simulation of anisotropic diffusion processes in fluids with smoothed particle hydrodynamics, Int. J. Numer. Methods Fluids 82 (11) (2016) 730–747.
[32] C.E. Alvarado-Rodríguez, L.D.G. Sigalotti, J. Klapp, Anisotropic dispersion with a consistent smoothed particle hydrodynamics scheme, Adv. Water Resour. 131 (2019) 103374.
[33] J. Klapp, L.D.G. Sigalotti, C.E. Alvarado-Rodríguez, O. Rendón, L. Díaz-Damacillo, Approximately consistent sph simulations of the anisotropic dispersion of a contaminant plume, Comput. Part. Mech. 9 (2022) 987–1002.
[34] S. Li, W.K. Liu, Moving least-square reproducing kernel method part II: Fourier analysis, Comput. Methods Appl. Mech. Eng. 139 (1–4) (1996) 159–193.
[35] W.K. Liu, S. Li, T. Belytschko, Moving least-square reproducing kernel methods I methodology and convergence, Comput. Methods Appl. Mech. Eng. 143 (1) (1997) 113–154.
[36] J. Bonet, T.S. Lok, Variational and momentum preservation aspects of smooth particle hydrodynamic formulations, Comput. Methods Appl. Mech. Eng. 180 (1–2) (1999) 97–115.
[37] N.J. Quinlan, M. Basa, M. Lastiwka, Truncation error in mesh-free particle methods, Int. J. Numer. Methods Eng. 66 (13) (2006) 2064–2085.
[38] J. Chen, J. Beraun, C.J. Jih, An improvement for tensile instability in smoothed particle hydrodynamics, Comput. Mech. 23 (4) (1999) 279–287.
[39] M.B. Liu, G.R. Liu, Restoring particle consistency in smoothed particle hydrodynamics, Appl. Numer. Math. 56 (1) (2006) 19–36.
[40] G.M. Zhang, R.C. Batra, Modified smoothed particle hydrodynamics method and its application to transient problems, Comput. Mech. 34 (2) (2004) 137–146.
[41] G.M. Zhang, R.C. Batra, Symmetric smoothed particle hydrodynamics (SSPH) method and its application to elastic problems, Comput. Mech. 43 (3) (2009) 321–340.
[42] Q. Zhu, L. Hernquist, Y. Li, Numerical convergence in smoothed particle hydrodynamics, Astrophys. J. Lett. 800 (1) (2015) 1–13.
[43] L.D.G. Sigalotti, O. Rendón, J. Klapp, C.A. Vargas, F. Cruz, A new insight into the consistency of the SPH interpolation formula, Appl. Math. Comput. 356 (2019) 50–73.
[44] D.J. Price, Modelling discontinuities and Kelvin-Helmholtz instabilities in SPH, J. Comput. Phys. 227 (24) (2008) 10040–10057.
[45] S. Ruiz-Bonilla, J. Borrow, V.R. Eke, J.A. Kegerreis, R.J. Massey, T.D. Sandnes, L.F.A. Teodoro, Dealing with density discontinuities in planetary SPH simulations, Mon. Not. R. Astron. Soc. 512 (3) (2022) 4660–4668.
[46] D.A. Fulk, D.W. Quinn, An analysis of 1-D smoothed particle hydrodynamics kernels, J. Comput. Phys. 126 (1) (1996) 165–180.
[47] J.J. Monaghan, J.C. Lattanzio, A refined particle method for astrophysical problems, Astron. Astrophys. 149 (1) (1985) 135–143.
[48] S. Shao, E.Y. Lo, Incompressible SPH method for simulating Newtonian and non-Newtonian flows with a free surface, Adv. Water Resour. 26 (7) (2003) 787–800.
[49] X. Zheng, Q. Ma, S. Shao, Study on SPH viscosity term formulations, Appl. Sci. 8 (2) (2018) 249.